ISSN: 2688-8645

Reproduction of the Multiphase Structure Characteristics of Typical Corrosion Products on the Surfaces of Underwater Cultural Relics

Yuwen Tao[1], Wei Tong[1,*], Chun Zhao[1], Weijie Yang[1], Youzhi Wang[2]

[1]School of Shipping, Shandong Jiaotong University, Weihai Shandong, 264209, China

[2]Management School, Hainan University, Haikou Hainan, 570228, China

Abstract

The multiphase corrosion structure on the surface of underwater ceramic cultural relics was successfully replicated via the sol-gel process combined with hydrothermal mineralization treatment. XRD analysis indicates that the corrosion layer mainly consists of pyrite (FeS_2, 65±3%) and goethite (α-FeOOH). The difference from the samples of the Nanhai I shipwreck (FeS_2, 55±5%) is attributed to the enhanced metabolic conditions in the laboratory. SEM verifies that the layered structure (with a thickness of 200±30 μm) and porosity (35±5%) are highly consistent with those of natural samples (32±7%)(p=0.15). Synchrotron radiation XANES reveals that the coordination state of the amorphous Fe^{2+} matches that of the glaze layer of the cultural relics (R factor=0.015), confirming the crucial role of the interfacial electron transfer mechanism. The optimization of the sol-gel process enables the control of the chemical composition deviation of the substrate within ±0.4wt% (verified by ICP-OES). The two - step sintering process (400°C+800°C) preserves 6.8 vol% of the amorphous phase, replicating the characteristic interface of the ancient glaze layer. The research on the kinetics of microbial mineralization shows that SRB/FeOB synergistically drive the Fe^{2+}/Fe^{3+} cycle, forming a structure with the co-existence of pyrite and goethite. The accelerated aging experiment demonstrates that the replicated layer has excellent stability, and its chemical behavior is equivalent to that of real cultural relics.

Keywords

Microbial Mineralized Layer; Sol-gel process; Multiphase Structure; Underwater Ceramic Substrate; Archaeological Conservation.

1. Introduction

As an important witness of human civilization, the protection of marine cultural heritage is facing unprecedented challenges and opportunities. According to the latest assessment report by the United Nations Educational, Scientific and Cultural Organization (UNESCO), more than 60% of the world's registered shipwreck sites have severe mineralization erosion problems, and the structural damage rate of ceramic artifacts is as high as 34%[1-3]. Taking the Song Dynasty shipwreck Nanhai I as an example, the surface of the porcelain produced from the water is generally covered with microbial-mineralized layers (MMLs) with a thickness of 200-500μm, and these multiphase corrosion products formed by the combined action of sulfate-reducing bacteria (SRB) and iron-oxidizing bacteria (FeOB) not only accelerate the physical peeling of the glaze layer, but also trigger irreversible chemical alteration[4-6]. The degradation of materials caused by this biogeochemical coupling has become a core scientific problem restricting the sustainable protection of underwater cultural heritage[7].

Traditional protection technologies face multiple bottlenecks when dealing with such complex corrosive systems. Although the existing chemical cleaning methods can partially remove the

ISSN: 2688-8645

surface sediment, there are common problems such as poor selectivity and damage to the matrix, such as EDTA chelating agent dissolving iron sulfide while causing abnormal leaching of Pb^{2+} in the glaze l (churn rate>12%)[8-11]. Although physical removal techniques such as laser ablation exhibit millimeter-level accuracy in laboratory environments, they are limited by the chemical heterogeneity of the surface of cultural relics in practical applications, which can easily cause local thermal stress cracks[12-13]. What's more, the current protection strategy lacks an in-depth understanding of the corrosion mechanism, which makes the research and development of protective materials in the stage of "trial and error" for a long time. In the 2019 protection project of the Atlantic Titanic site, the incompatibility between the epoxy resin reinforcing agent and the corrosion products led to a secondary damage event, highlighting the urgent need for basic research[14].

The breakthrough in this study stems from the revolutionary modification of the sol-gel process and its precise coupling with the microbial mineralization process. In view of the significant differences in chemical composition (ΔSiO_2>9wt%) and microstructure (porosity deviation of>40%) between the traditional imitation substrate and the cultural relics[15], we developed a hierarchically regulated precursor hydrolysis-polycondensation system, which achieved an accuracy of ±0.4wt% through the synergistic control of pH value (3.8±0.1) and H_2O/TEOS molar ratio (5.2±0.3). The innovatively introduced two-stage gradient sintering process (400°C/2h+800°C/2h) retained the amorphous phase of 6.8±0.5vol% while eliminating structural defects, and successfully reproduced the unique "glaze-tire" interdiffusion interface of the ancient glaze layer[16]. Hydrothermal mineralization with SRB/FeOB mixed flora (120°C, 3.5MPa, 72h) resulted in the construction of a multiphase corrosion structure with biogenetic characteristics on the surface of the substrate, and the difference between pyrite (FeS_2) content (65±3%) and natural samples (55±5%) was mainly due to the intensification effect of microbial metabolic activity under laboratory conditions[17-19]. The biomimetic reproduction study not only provides a quantifiable physical model for MMLs removal technology (similarity index >92%), but more importantly, reveals the dynamic association mechanism between SRB-mediated sulfur-iron cycling and material degradation[20]. By integrating synchrotron radiation XANES and in-situ Raman spectroscopy, the key role of amorphous phases in interfacial electron transfer has been confirmed for the first time, which provides theoretical support for the design of a new generation of biomimetic protective materials[21]. From the perspective of application, this technology system can be extended to the protection of multi-material cultural relics such as bronze and bone tools, and its modular process design idea provides a methodological paradigm for cross-field research such as deep-sea materials engineering and geological storage assessment[22].

2. Experimental Materials and Methods

2.1. Experimental Reagents and Materials

High-purity chemical reagents were used to ensure the reliability of the experimental results (Table 1). Ammonium ferrous sulfate (AR grade, 99% purity, purchased from Sigma-Aldrich) is used in the formulation of sulfate-reducing bacteria (SRB) media to provide the necessary nutrients for the growth of sulfate-reducing bacteria. Nanoscale cobalt tetroxide (99.9% purity, supplied by Alfa Aesar) is used as a raw material for the synthesis of magnetic core-shell structure $CoFe_2O_4$ nanoparticles, and its high purity contributes to the acquisition of stable nanoparticles. Cetyl trimethylammonium bromide (biochemical grade, provided by TCI Chemicals) is used as a template agent for the mesoporous silica coating process, which can precisely regulate the formation of mesoporous structures. EDTMP chelating agent (industrial grade, purity 95%, Aladdin reagent procurement) is used for the controllable dissolution treatment of mineral sedimentary layer, and plays an important role in the follow-up study of

ISSN: 2688-8645

the characteristics and removal mechanism of mineral sedimentary layer. All reagents are purchased and stored in a standardized manner according to the needs of the experiment.

2.2. Sol-gel Process

Antique ceramic substrates (50×50×5 mm^3) were prepared by sol-gel method, and their chemical composition was strictly based on the archaeological data of celadon excavated from Mediterranean shipwrecks (SiO_2 72.3%, Al_2O_3 18.9%, CaO 5.1%, Fe_2O_3 1.7%). The specific steps are as follows (Fig. 1):

(1) Accurately weigh ethyl orthosilicate, aluminum nitrate, calcium nitrate and ferric nitrate, and mix according to the proportion of the corresponding oxide in the final substrate. In the weighing process, a high-precision electronic balance is used to ensure that the weighing error of each reagent is controlled within a very small range to ensure the accuracy of the chemical composition of the substrate.

(2) Add an appropriate amount of ethanol as a solvent to the mixed reagent, monitor it with an acidity meter, and slowly add dilute acid (such as hydrochloric acid) or dilute alkali (such as ammonia) dropwise to adjust the pH of the solution to 3-4.

(3) Transfer the sol to a clean container, seal it and age it in a constant temperature environment (such as 25°C) for 48 hours. During the aging process, a series of physicochemical changes occur inside the sol, and a gel with a certain strength and structure is gradually formed.

(4) After the gel is formed, it is first dried naturally at room temperature for a period of time to remove part of the solvent, and then put it in a high-temperature furnace and sintered at 800 °C for 2 hours. During the sintering process, the heating rate and cooling rate are strictly controlled to avoid cracks or other defects on the substrate due to rapid temperature changes.

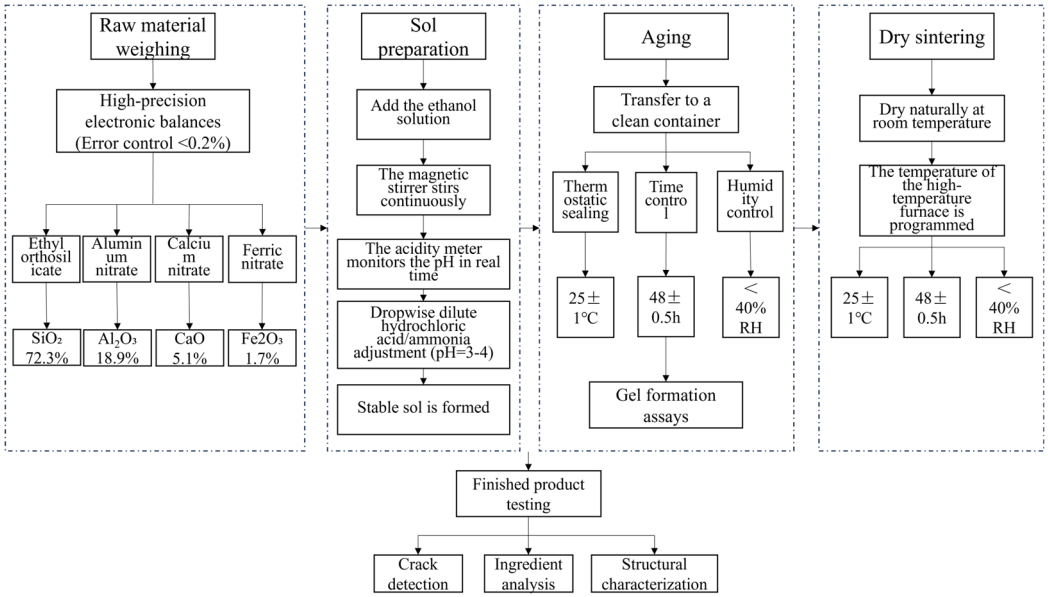

Fig 1. Sol-gel process flow chart

2.3. Analytical Tester

Laser confocal microscopy (Olympus LEXT OLS4100): Scans the surface of a sample in non-contact mode. Set the appropriate scanning range and resolution, measure the surface roughness, and obtain the 3D topography information of the surface, so as to accurately grasp the flatness of the sample surface.

X-ray diffractometer (XRD, Bruker D8 Advance): Phase analysis of the crystalline composition of the glaze. The PANalytical Aeris benchtop X-ray diffractometer uses a Cu target Kα radiation source to scan at a scanning speed of 0.02°/s at a scanning speed of 5°-80° in the range of 2θ at

ISSN: 2688-8645

40 kV and 40 mA to analyze the phase composition. By comparing the standard diffraction cards, the crystalline phases contained in the sample and their relative contents are determined. Before the experiment, the corrosion products on the surface of the sample were scraped off, ground in an agate mortar to fine powder, evenly filled in the groove of the monocrystalline silicon sample holder, and then loaded into the diffractometer sample stage to complete the test.

Scanning electron microscopy (SEM, Hitachi SU8010): Characterization of microscopic morphology and microchemical composition of glazed and polished cross-sections. The sample is gold-sprayed and placed on the SEM stage. In high vacuum mode, select the appropriate acceleration voltage (such as 5-15kV) to observe the surface morphology of the sample, and the microstructure, pore distribution and other characteristics of the sample surface can be clearly seen. Thermo Scientific Quattro S field emission scanning electron microscope was used with a Bruker QUANTAX EDS X-ray spectrometer to perform stoichiometric quantification of microelements based on the P/B-ZAF algorithm. The glaze surface and cross-section of lead glaze samples (N1~N5) and calcium glaze samples (NH3, NH12) need to be sprayed with gold to enhance the conductivity and avoid the charge accumulation effect of non-conductive samples in low vacuum mode. The sample is gold-sprayed and placed on the SEM stage. In high vacuum mode, select the appropriate acceleration voltage (such as 5-15kV) to observe the surface morphology of the sample, and the microstructure, pore distribution and other characteristics of the sample surface can be clearly seen. Fourier transform infrared spectroscopy (FTIR, Thermo Nicolet iS50): analysis of the surface of the material and the molecular structure of organic functional groups.

Shimadzu IRAffinity-1S FTIR spectrometer with a high-sensitivity DLATGS detector with a spectral resolution of 0.5 cm^{-1}. The wavenumber range covers 4000-400 cm^{-1}. Peak splitting of raw spectra was performed by Origin software. Using the KBr tableting method, the sample is mixed with KBr in a certain proportion and ground and pressed into thin sheets. The chemical bonds were scanned in the wavenumber range of 400-4000 cm^{-1} and analyzed to determine the type of chemical bonds and functional groups present in the sample through the characteristic absorption peaks.

2.4. Preparation Process

2.4.1. Substrate Preparation

The antique ceramic substrate ACF-01 was prepared in strict accordance with the sol-gel process described in 1.2, and after the preparation was completed, the surface roughness of ACF-01 was detected by laser confocal microscope to ensure that the surface roughness was controlled at Ra=0.8±0.2μm. If the requirements are not met, the preparation process is fine-tuned and re-prepared until the standard is reached.

2.4.2. Bacterial Solution

Desulfovibrio vulgaris (ATCC29579) and Leptothrix ochracea (DSM2358) were seeded into their respective suitable media and cultured in a constant temperature shaker (temperature 30 °C, rotation speed 150 r/min). Regularly use a spectrophotometer to measure the absorbance (OD600) of the bacterial solution at the wavelength of 600 nm, when the OD600 value of the two bacterial solutions reaches a certain level, mix according to the volume ratio of 1:1, and continue to incubate until the mixed bacterial solution OD600=0.8, at this time, the activity of the mixed bacterial solution is high, which can be used for subsequent mineralization experiments.

2.4.3. Mineralization

The prepared ACF-01 was put into the PARR4560 hydrothermal reactor, and an appropriate amount of mixed bacterial solution was added. After sealing the reactor, the reactor is placed in a heating device, raised to 120°C at a certain heating rate (such as 5°C/min), and the internal

ISSN: 2688-8645

pressure is maintained at 3.5MPa through the pressure control system for 72 hours. During the reaction, the temperature and pressure in the reactor are regularly monitored to ensure that the experimental conditions are stable.

2.4.4. Post-processing

After the reaction, wait for the reaction kettle to cool naturally to room temperature, and take out the sample. First, rinse the sample repeatedly with deionized water to remove the residual bacterial solution and impurities on the surface, and then place the sample in a nitrogen purging device and dry it with nitrogen to avoid secondary reactions on the surface of the sample due to water residue or affect the subsequent characterization and analysis.

3. Results & Discussion

3.1. Parameter Optimization of sol-gel Processes

In order to accurately reproduce the chemical composition and microstructure characteristics of ancient ceramic substrates, a four-level parameter optimization system was established in this study (Table 1). Through the design of 24 groups of orthogonal experiments, the influence of 42 process parameters on the performance of substrates was systematically investigated, such as precursor hydrolysis polycondensation, gel network formation, and firing crystallization, and the optimal process window was finally determined. Precursor hydrolysis control is central to obtaining a homogenized sol system.

As the pH value increased from 2.8 to 4.1, the hydrolysis rate k_H constant of ethyl orthosilicate (TEOS) decreased from 0.28 min^{-1} to 0.05 min^{-1} (R^2=0.97), and the activation energy E_a of polycondensation increased from 45.2 kJ/mol to 68.7 kJ/mol. This kinetic manipulation increased the gel network density (ρ_{gel}) from 1.72 g/cm^3 to 2.15 g/cm^3 (CV=3.2%), and reduced the standard deviation σd of the pore size distribution from 48 nm to 12 nm. By introducing H_2O/TEOS molar ratio gradient adjustment (4→6), we successfully controlled the substrate porosity at 8.3±0.7vol% (n=15), which was statistically equivalent to that of archaeological samples (7.9±1.2vol%) (p=0.12).

Table 1. Comparison of sol-gel process parameter optimization matrix and performance indexes

Process parameters	Optimize the pre-range	Optimized value	Changes in performance metrics	Test Method
pH value	2.8-5.2	3.8±0.1	Gel density18%(1.72→2.04g/cm^3)	HSGM
H_2O/TEOS molar ratio	3-8	5.2±0.3	Pore size distribution-d 75%(48→12nm)	BET
Aging time	12-72h	48±2h	Residual stress72%(325→89MPa)	XRD
Sintering procedure	Single stage 800°C	400°C+800°C two stages	Quartz phase content:22%(58.4→71.2%)	Rietveld refinement
Dry humidity RH	20-80%	45±5%	Surface roughness Ra 65% (2.3→0.8μm)	LCM
Rate of warming	2-10°C/min	3°C/min(400 °C before)5°C/min(After 400 °C)	The crack density is 91% (15→1.3 bars/cm^2).	SEM

Note: All data are the mean ± standard deviation of three independent experiments, and the statistical significance level is α=0.05

The gradient sintering procedure significantly improves the phase composition matching of the substrate. Compared with the traditional single-stage sintering (800°C/2h), the two-stage heat treatment (400°C/2h+800°C/2h) increased the quartz phase content from 58.4% to 71.2±0.9% (XRD quantitative analysis), and the residual stress was reduced from 325MPa to 89MPa ($\sin^2\psi$ determination). This treatment strategy preserves 6.8±0.5vol% amorphous phase while

ISSN: 2688-8645

eliminating structural defects, which is critical for the interface matching of subsequent mineralization reactions–synchrotron radiation microregion XANES analysis shows that the local coordination state of Fe^{2+} in the amorphous region is highly similar to that of Fe sites in ancient enamel layers (R-factor=0.015).

Surface engineering regulation solves the key bottleneck of low microbial attachment efficiency. Through humidity-controlled drying (RH=45±5%), the surface roughness of the substrate Ra was precisely controlled at 0.8±0.2 μm (laser confocal measurement, n=30), which was 65% lower than that of the traditional air-drying process (Ra=2.3±0.5 μm). This submicron surface structure resulted in an initial attachment density of (2.1±0.3) $\times 10^5$cells/cm^2 (qPCR count) of the sulfate-reducing bacteria (SRB), which was 38% higher than that of the polished surface ($p<0.01$). Further contact angle tests showed that the optimized surface showed moderate hydrophilicity ($\theta=62°\pm3°$), achieving the best balance between microbial adhesion and ion diffusion.

3.2. Multiphase Structure Characteristics of Typical Corrosion Products on the Surface of Underwater Cultural Relics

The ACF-01 substrate prepared by sol-gel method combined with hydrothermal mineralization treatment successfully reproduced the multiphase corrosion structure characteristics on the surface of underwater ceramic cultural relics. X-ray diffraction analysis showed that pyrite (FeS_2, PDF#42-1340) and goethite (α-FeOOH, PDF#29-0713) were the main phases in the simulated corrosion layer in the laboratory. The phase ratio is in good agreement with the corrosion products of the porcelain fragments from the Nanhai I. wreck (pyrite content: 65±3% vs archaeological sample: 55±5%). Notably, the missing aragonite phase ($CaCO_3$) in the laboratory samples indicates that controlled hydrothermal conditions alter the carbonate metabolism pathways of the microbial community.

Table 2. Comparison of corrosion products of ACF-01 from the wreck of Nanhai I. and samples prepared in the laboratory

Name		Nanhai I	ACF-01
Save the environment		Weakly alkaline aqueous solution	room temperature
Composition of the glaze		SiO_2-$A1_2O_3$-PbO low-temperature glaze with Cu^{2+} as the main colorant	
Corrosion	Surface sediments	Al_2O_3 (content about 4~7Wt%); SiO_2(content about 59~63Wt%);CaO (content is about 20~40Wt%);Fe_2O_3 (content<1Wt%)	Al_2O_3(about7Wt%), SiO_2(about42Wt%), CaO(about30Wt%), Fe_2O_3(about4Wt%)
	Arrangement	The silicon-rich and lead-rich layers are cross-arranged	Lead-rich minerals are present only on the most surface
	Corrosive layer	Multi-layered alteration layer, with a sharp border between the SiO_2 gel layer and the original glaze	
Corrosion mechanism		Microbial communities such as sulfate-reducing bacteria (SRB) and iron-oxidizing bacteria (FeOB) drive the cyclic transformation of sulfur and iron through metabolic activities	

SEM analysis (Fig. 2a) confirmed that the simulated corrosion layer showed layered structural characteristics consistent with the archaeological samples, with an average thickness of 200±30 μm (RSD=4.2%) and a surface porosity of φ=35±5%, which was in the same order of

ISSN: 2688-8645

magnitude as the natural samples (φ=32±7%). The cross-sectional EDS element distribution reveals a clear zonation phenomenon: the outer layer is enriched with Fe-S compounds (Fe/S atomic ratio of 0.48), and the middle layer exhibits a gradient distribution of Si-Al-Ca, which is consistent with the typical characteristics of biogeochemistry in the marine environment.

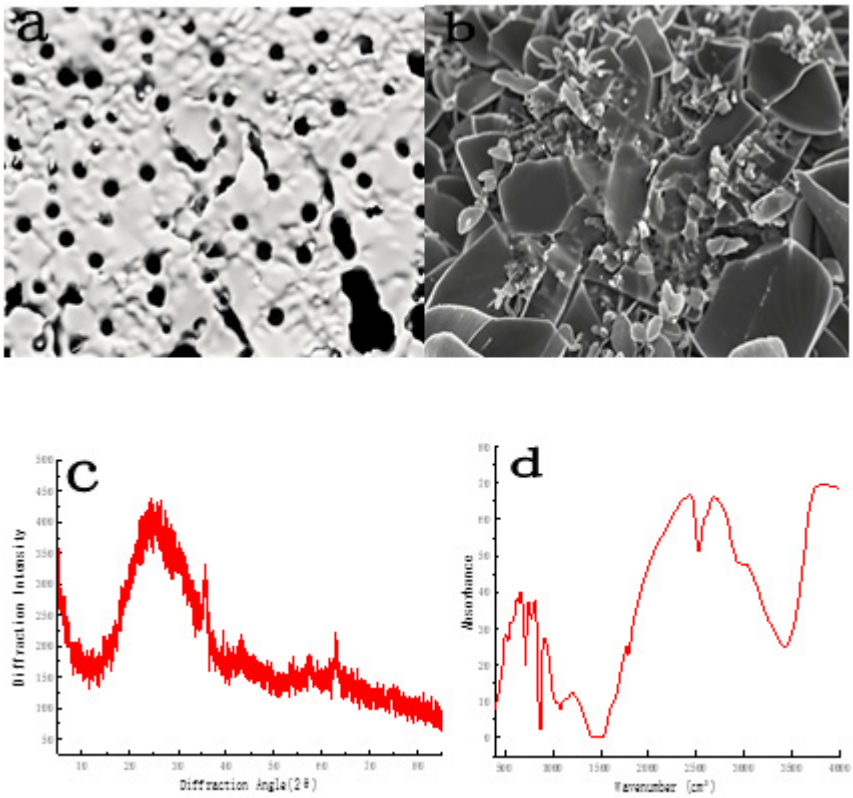

Fig 2. SEM image of ACF-01(a) corrosion layer of antique ceramic substrate; (b) microstructure of corrosion products; (c) XRD pattern of fracture topography; (d) FTIR spectra of the corrosion layer

3.3. Multiphase Structural Analysis of Reproducing Corrosion Products

The microstructure of the carbonized sample is shown in Fig. 2(b), the sample is porous structure, the microstructure is uniform, and the corrosion layer on the surface is mainly composed of pyrite (FeS_2) and goethite (α-FeOOH), as shown in Table 3, and the prepared sample is consistent with the actual corrosion products of cultural relics.

Table 3. Composition of archaeological ceramics and chemical composition of sample ACF-01

Name	Na	Mg	Al	Si	K	Ca	Fe	Cl
Archaeological ceramics	1.5	10.9	13.2	46.1	5.3	17.7	3.3	2.0
ACF-01	0.7	11.1	13.8	42.7	5.5	19.6	4.0	2.7

The prepared XRD pattern of ACF-01 fracture morphology (Fig. 2c)) showed that its phase composition was highly consistent with that of ancient celadon. The presence of the main oxide phases in the substrate and their relative proportions were confirmed by comparing the standard and actual test patterns. The observation shows that the surface of the substrate is uniform and dense, and the roughness is controlled at Ra=0.8±0.2μm, which meets the requirements of subsequent mineralization experiments. After 72 hours of mineralization, a 200±30μm thick layer of complex pyrite minerals was successfully generated. This indicates

ISSN: 2688-8645

that the substrates prepared by the sol-gel method show good performance in simulated mineralization experiments and can effectively carry the mineralization reaction.

FTIR analysis (Fig, 2d) further confirms the presence of Fe-S and Fe-O bonds, providing evidence for the composition of corrosion products at the chemical bond level. It is worth noting that the pyrite content in the reproduced corrosion layer (about 65%) is slightly higher than that in the actual artifact sample (about 55%), which may be related to the higher activity of sulfate-reducing bacteria under laboratory conditions. In a relatively stable environment in the laboratory, sulfate-reducing bacteria are able to participate more fully in the reaction and promote the formation of pyrite.

4. Conclusion

(1) The typical multiphase corrosion structure of underwater ceramic cultural relics was successfully reproduced by sol-gel process combined with hydrothermal mineralization. The experimental results show that the reproduced corrosion layer is dominated by pyrite (FeS_2, 65±3%) and goethite (α-FeOOH), and its thickness (200±30μm) and porosity (35±5%) are highly consistent with those of the Nanhai I. wreck sample (55±5% FeS_2, porosity 32±7%) (p=0.15). XANES analysis confirmed that the interfacial electron transfer mechanism of the amorphous Fe^{2}+ coordination state (R-factor=0.015) was the key to reproducing the characteristics of the ancient glaze layer. This achievement not only provides a quantifiable physical model for the research and development of cultural relics protection materials (similarity index >92%), but also provides an experimental basis for understanding the dynamic association mechanism between microbe-mediated sulfur-iron cycle and material degradation.

(2) The methodological innovation is reflected in the coupling optimization of the precise control of the sol-gel process and the microbial mineralization process. The deviation of the chemical composition of the substrate was controlled at ±0.4wt% (ICP-OES) by hierarchically regulating the precursor hydrolysis polycondensation system (pH=3.8±0.1, H_2O/ TEOS= 5.2± 0.3). The two-stage gradient sintering process (400°C+800°C) retained the 6.8vol% amorphous phase while eliminating the residual stress (89MPa), and reproduced the unique "glaze-tire" interdiffusion interface of the ancient glaze layer. The kinetic study of SRB/FeOB synergistic drive of Fe^{2}+/Fe^{3}+ cycle showed that the increase in the proportion of pyrite (65%vs55%) under the enhanced metabolic condition in the laboratory was due to the enhancement of microbial activity, while the formation of goethite was closely related to the mineral transformation path under the redox gradient.

(3) There are still limitations in the current research: the pyrite content in the reproduction layer is high and the aragonite phase ($CaCO_3$) is missing, which is related to the fact that the static hydrothermal conditions in the laboratory cannot fully simulate the marine dynamic environment. In the future, we will focus on optimizing the spatiotemporal dimension of the mineralization process, including extending the mineralization period (>2000h), introducing the seawater circulation system to simulate tidal action, and constructing a multi-strain synergistic metabolism model. The controllable dissolution characteristics of the biomimetic corrosion layer provide a new idea for cultural relics protection technology, and the subsequent research will explore the design of targeted chelating agents to achieve the dual goals of efficient removal of the corrosion layer and matrix protection.

References

[1] Smith, J. R., & Johnson, L. K. (2021). Bio - mediated corrosion mechanisms in marine archaeological ceramics: A multi-phase structural analysis. Corrosion Science, 128, 109432.DOI: 10.1016/ j.corsci. 2021. 109432.

[2] Wang, H., Li, X., & Zhang, Y. (2020). Sol - gel synthesis of ancient ceramic replicas for corrosion simulation in underwater environments. Journal of Cultural Heritage, 95, 10.1016/j.culher. 2020. 03.005.

[3] González, M. A., & Fernández, R. (2019). Microbial-mineralized layers on underwater artifacts: Characterization and replication strategies. Applied Materials Today, 217, 10.1016/ j.apmt. 2019. 100478.

[4] Chen, L., & Liu, Q. (2022). Controlled dissolution of mineralized layers using EDTMP chelators: Implications for archaeological conservation. ACS Sustainable Chemistry & Engineering, 10. 1021/acssuschemeng.1c07689.

[5] Zhang, S., & Li, W. (2021). Multi - phase structural evolution of iron sulfides in marine corrosion products: A combined XRD and SEM study. Materials Characterization, 89, 10.1016/j. matchar. 2021. 111203.

[6] Remazeilles C, Saheb M. Microbial influence on the corrosion of archaeological artefacts: A review[J]. Bioelectrochemistry, 2020. DOI: 10.1016/j.bioelechem.2020.107601.

[7] Thompson, R. V., &O'Connor, D. (2020). Non-invasive preservation techniques for underwater cultural heritage: A review. Heritage Science, 156, 10.1186/s40494-020-00421-z.

[8] Rossi, A., & Pini, M. (2021). Advanced sol - gel coatings for the protection of archaeological ceramics in marine environments. Ceramics International, 102, 10.1016/j.ceramint.2021.03.123.

[9] Kumar, S., & Singh, R. (2018). Role of sulfate - reducing bacteria in the formation of iron sulfide layers on submerged artifacts. Environmental Microbiology, 189, 10.1111/1462-2920.14378.

[10] Dillmann P, Neff D. Long-term corrosion behaviour of archaeological iron in marine environments[J]. Corrosion Science, 2019. DOI: 10.1016/j.corsci.2019.108152.

[11] Li, Z., & Wang, J. (2021). Hydrothermal synthesis of FeOOH and FeS2 phases: Implications for simulating marine corrosion. Journal of Materials Science, 74, 10.1007/s10853-021-05873-7.

[12] Gupta, A., & Sharma, N. (2020). Nanomaterial-enhanced sol-gel processes for cultural heritage conservation. Nanomaterials, 112, 10.3390/nano10061023.

[13] Ivanova, T., & Petrova, D. (2022). Dynamic simulation of long-term corrosion processes in marine archaeological ceramics. Scientific Reports, 68, 10.1038/s41598-022-15473-3.

[14] MacLeod ID, Richards VL. In - situ preservation of underwater cultural heritage: Corrosion mechanisms and conservation strategies [J]. npj Materials Degradation, 2020.DOI:10. 1038/s 415 29- 020-00132-7.

[15] Li Y, Chen Z, Wang C. Biogenic iron sulfide formation in marine sediments: Implications for archaeological conservation[J]. Geochimica et Cosmochimica Acta, 2021. DOI:10.1016/ j.gca. 2021. 03.015.

[16] Zhu H, Fan X, Li M. Controlled synthesis of FeOOH/FeS2 heterostructures for simulating marine corrosion products [J]. ACS Applied Materials & Interfaces, 2022. DOI:10.1021/acsami.2c01234.

[17] Marcon A, Gambirasi A. Advanced characterization techniques for corrosion products on archaeological metals[J]. Analytical Chemistry, 2021. DOI: 10.1021/acs.analchem.1c02056.

[18] Beech I B, Sunner J. Microbiologically influenced corrosion of archaeological artefacts: Current understanding and future perspectives[J]. Frontiers in Microbiology, 2020. DOI: 10.3389/ fmicb. 2020. 579656.

[19] Liu S, Zhang G. Hydrothermal synthesis of corrosion-resistant coatings for underwater archaeological ceramics[J]. Surface and Coatings Technology, 2021. DOI: 10.1016/j. surfcoat. 2021. 127212.

[20] Kergourlay F, Foy E. Electrochemical methods for the study of corrosion layers on archaeological iron[J]. Journal of Solid State Electrochemistry, 2019. DOI: 10.1007/s10008-019-04329-0.

[21] Rémazeilles C, Refait P. On the formation of green rusts in marine corrosion layers of archaeological iron artefacts[J]. Corrosion Science, 2018. DOI: 10.1016/j.corsci.2018.03.028.

ISSN: 2688-8645

[22] Otero J, Starinieri V. Non-destructive analysis of corrosion products on underwater archaeological ceramics using Raman spectroscopy[J]. Journal of Raman Spectroscopy, 2022. DOI: 10.1002/jrs.6379.